International Journal of Biological Macromolecules 163 (2020) 375–385

Contents lists available at ScienceDirect

International Journal of Biological Macromolecules

journal homepage: http://www.elsevier.com/locate/ijbiomac

# Guanidinium binding to proteins: The intriguing effects on the D1 and D2 domains of *Thermotoga maritima* Arginine Binding Protein and a comprehensive analysis of the Protein Data Bank

Serena Cozzolino [a], Nicole Balasco [b], Marilisa Vigorita [c], Alessia Ruggiero [b], Giovanni Smaldone [d], Pompea Del Vecchio [a], Luigi Vitagliano [b], Giuseppe Graziano [c,*]

[a] Department of Chemical Sciences, University of Naples Federico II, via Cintia, 80126 Napoli, Italy
[b] Institute of Biostructures and Bioimaging, CNR, Via Mezzocannone 16, I-80134 Napoli, Italy
[c] Department of Science and Technology, University of Sannio, via Francesco de Sanctis snc, Benevento 82100, Italy
[d] IRCCS SDN, Via Emanuele Gianturco, 113, 80143 Napoli, Italy

ARTICLE INFO

*Article history:*
Received 24 May 2020
Accepted 30 June 2020
Available online 04 July 2020

*Keywords:*
Protein stability
Guanidinium chloride denaturation
Guanidinium binding to proteins

ABSTRACT

*Thermotoga maritima* Arginine Binding Protein has been extensively characterized because of its peculiar features and its possible use as a biosensor. In this characterization, deletion of the C-terminal helix to obtain the monomeric protein TmArgBP$^{20-233}$ and dissection of the monomer in its two domains, D1 and D2, have been performed. In the present study the stability of these three forms against guanidinium chloride is investigated by means of circular dichroism and differential scanning calorimetry measurements. All three proteins show a high conformational stability; moreover, D1 shows an unusual behavior in the presence of low concentrations of guanidinium chloride. This finding has led us to investigate a possible binding interaction by means of isothermal titration calorimetry and X-ray crystallography; the results indicate that D1 is able to bind the guanidinium ion ($GuH^+$), due to its similarity with the arginine terminal moiety. The analysis of the structural and dynamic properties of the D1-$GuH^+$ complex indicates that the protein binds the ligand through multiple and diversified interactions. An exhaustive survey of the binding modes of $GuH^+$ to proteins indicates that this is a rather common feature. These observations provide interesting insights into the effects that $GuH^+$ is able to induce in protein structures.



## 1. Introduction

The Arginine Binding Protein isolated from *Thermotoga maritima* (TmArgBP) is a member of the Substrate Binding Proteins (SBPs) family, a group of proteins which interact with the bacterial ATP-Binding Cassette (ABC) system, responsible of the transportation of molecules across the periplasmic membrane [1].

TmArgBP has been extensively studied not only for its possible use as a biosensor but also for its peculiar structural features [2–9]. It specifically binds arginine, with a dissociation constant ($K_D$) of 1.3 ± 0.9 nM [8], and is highly thermostable, having a denaturation temperature ($T_d$) of 114.9 ± 0.3 °C in the ligand-free form [5], despite its loose domain swapped dimeric structure [8]. Given these characteristics, it is a promising scaffold for an arginine biosensor, as already described in the literature [5,6,8,10–12]. Moreover, the studies conducted so far have shed light on important topics such as domain swapping [13] [14], structure/function relationships [8,10], stability/flexibility issues [15].

In one of the more recent publications on TmArgBP [10], a dissection of the protein in its two major domains, named D1 and D2, is presented. The domains are studied for their thermal stability and ability to interact with arginine, and are compared to TmArgBP$^{20-233}$, the truncated form of the wild-type protein, in which the terminal swapping helix is deleted to obtain a monomeric structure; D1 has a binding site for the arginine, and retains a good affinity for this ligand, while the isolated D2 does not interact with it, despite its cooperation in substrate binding in the wild-type protein. Nevertheless, D2 presents a high thermal stability and represents an interesting system to investigate stability-structure relationships in proteins [10].

To continue the study of the thermodynamics of these domains, whose conformational stability against temperature has already been

*Abbreviations:* TmArgBP, wild-type Arginine Binding Protein isolated from *Thermotoga maritima*; TmArgBP$^{20-233}$, residues 20–233 of TmArgBP; D1, domain 1 of TmArgBP; D2, domain 2 of TmArgBP; SBP, substrate binding protein; GuHCl, guanidinium chloride; $GuH^+$, guanidinium ion; RMSD, root mean square deviation; RMSF, root mean square fluctuation; PDB, Protein Data Bank; CD, circular dichroism; RMSIP, root mean square inner product; DSC, differential scanning calorimetry; ITC, isothermal titration calorimetry; PBS, phosphate buffered saline.

* Corresponding author.
*E-mail address:* graziano@unisannio.it (G. Graziano).

https://doi.org/10.1016/j.ijbiomac.2020.06.290
0141-8130/

studied [10], the stability of TmArgBP$^{20–233}$ and its domains D1 and D2 against the denaturing action of guanidinium chloride (GuHCl) is here investigated. Two approaches have been used: (a) chemical denaturation of the protein samples is performed and recorded by means of circular dichroism (CD) measurements, and by analyzing data according to the linear extrapolation method [16]; (b) differential scanning calorimetry (DSC) experiments have been performed in the presence of different GuHCl concentrations. These experiments collectively show that both domains proved to be very stable against GuHCl, with a GuHCl concentration at half denaturation larger than 4 M and a denaturation temperature above 75 °C in aqueous solution with 2.5 M GuHCl. In addition, D1 has shown an unusual behavior as it is stabilized by low concentrations of GuHCl. Isothermal titration calorimetry (ITC) measurements and the determination of the crystal structure of D1 in the presence of GuHCl have provided a structural interpretation of this intriguing finding. Moreover, a comprehensive analysis of the Protein Data Bank (PDB) indicates that proteins and the guanidinium ion ($GuH^+$) interact through multiple and diversified interactions. The implications of this observation for interpreting the impact of this ion on protein structures are also discussed.

## 2. Materials and methods

### 2.1. Materials

Tris(hydroxymethyl)aminomethane hydrochloride (TrisHCl) and sodium chloride (NaCl) salts were purchased from Sigma-Aldrich. Phosphate salts ($NaH_2PO_4$ and $Na_2HPO_4$) were from J.T. Baker, while PBS (Phosphate Buffered Saline) tablets were from Life Technologies/Gibco. To prepare the buffer solutions, the salts were dissolved in Milli-Q (Millipore, Bedford, MA) water. Guanidinium chloride (GuHCl) was a ready-to-use 8 M buffered solution from Sigma Aldrich. Dialysis membranes (cut-off 6000–8000 Da) were from Spectrum Laboratories, Inc.

### 2.2. Protein cloning, expression and purification

TmArgBP$^{20–233}$, the monomeric form of the protein obtained by the deletion of the C-terminal helix, and its domains D1 (residues 20–114 and 207–233 linked by a GGGGSG segment) and D2 (residues 115–206) were expressed and purified as previously described [10,15]. The contructs of the domains D1 and D2 also bear a histidine rich tag with sequence LEHHHHHH at the C-terminus to improve the purification procedure. The D1 domain, which hosts most of the residues that cooperate for arginine binding, was purified in the arginine-bound form. To obtain the ligand-free form, D1 was dialyzed against 6 M GuHCl for two days and then the denaturant was removed by extensive dialysis in a buffer solution containing 50 mM TrisHCl and 150 mM NaCl, pH 8, for 5–6 days; D1 was finally purified using a Superdex S75 16/60 column, pre-equilibrated in the dialysis buffer.

Before the spectroscopic or calorimetric measurements, protein samples were dialyzed in PBS solution at pH 7.4, and their concentration after dialysis was obtained applying the Lambert-Beer equation by measuring the absorbance at 280 nm and considering the theoretical molar extinction coefficient calculated according to Pace et al. [17].

### 2.3. Circular dichroism spectroscopy

Circular dichroism (CD) spectra were recorded on a J-715 spectropolarimeter (Jasco Europe, Cremella (LC), Italy) equipped with a Peltier temperature control system. Measurements in the far-UV region (190–260 nm) were carried out at 25 °C using a 0.1 cm optical path length cell. The parameters were set as follows: 4 s response time, 2 nm bandwidth, 20 nm $min^{-1}$ scan rate; the signal was averaged over at least two scans.

Protein samples were diluted in 10 mM sodium phosphate buffer, pH 7.4 at a final concentration of 0.1 mg $mL^{-1}$. A buffer scan was recorded before each scan of protein samples.

To perform the chemical denaturation of each protein, 20 samples were prepared keeping constant the protein concentration, and increasing GuHCl concentration from 0 M to 7 M. The measurements were performed in duplicate for each species. Reversibility was checked by removing the denaturant by dialysis and repeating the CD measurements under the same conditions.

CD spectra were corrected by buffer subtraction and normalized per mole of residue. Denaturation curves were obtained by reporting the molar ellipticity at 222 nm as a function of GuHCl concentration. The sigmoidal curves were analyzed by means of the linear extrapolation model, LEM, fitted using a nonlinear least squares method, that assumes a linear dependence of the denaturation Gibbs energy change upon the denaturant concentration, i.e. $\Delta_d G = \Delta_d G(H_2O) - m[Den]$ [16]. According to Pace et al. [18], the following equation has been implemented in the Origin8 software package to perform a nonlinear regression:

$$y = \frac{(y_F^0 + m_F[Den]) + (y_U^0 + m_U[Den])\, exp\,((-\Delta_d G(H_2O) + m[Den])/RT)}{1 + exp\,((-\Delta_d G(H_2O) + m[Den])/RT)}$$

Here, y is the signal of interest (molar ellipticity at 222 nm, $[\theta]_{222}$, at different GuHCl concentrations); $y_F^0$ and $y_U^0$ indicate the intercepts of the pre- and post-denaturation lines; $m_F$ and $m_U$ the corresponding slopes; $m$ the slope of the curve in the transition region; [Den] the denaturant concentration at each point; R is the gas constant, equal to 8.314 J $mol^{-1}$ $K^{-1}$ and T is the temperature expressed in Kelvin. This approach allows the calculation of the value of the Gibbs energy change associated with the denaturation process in the absence of denaturant, $\Delta_d G(H_2O)$.

### 2.4. Differential scanning calorimetry

Differential scanning calorimetry (DSC) measurements were performed on a Nano-DSC (TA Instruments, New Castle, DE, USA) under a total pressure of 3 atm applied with nitrogen gas to both cells in the calorimeter, and using a scan rate of 1 °C $min^{-1}$. The samples were prepared at a concentration of 0.4 mg $mL^{-1}$ in a 2 mL calibrated flask, by mixing a suitable amount of protein and, where needed, denaturant and then adding PBS buffer until reaching the final volume. In this way any concentration error due to the different densities of the solutions is minimized. The samples were then degassed for 5 min before the measurements. Each measurement has been repeated twice; before each one, a blank (consisting of buffer or buffer plus GuHCl) was recorded using the same sample parameters so as to subtract contributions not due to the sample. All thermodynamic data are given per mole of protein (considering a molar mass of 23.7 kDa for TmArgBP$^{20–233}$, 15.3 kDa for D1 and 11.2 kDa for D2).

The Nano-Analyze software package supplied by the manufacturer has been used for data analysis. The excess molar heat capacity function, $<\Delta C_p>$, is obtained after a baseline subtraction, assuming that the baseline is given by the linear temperature dependence of the native-state heat capacity. The denaturation temperature, $T_d$, corresponds to the maximum of the DSC peak; the denaturation enthalpy change, $\Delta_d H$ ($T_d$), is the integrated area under the DSC peak. The uncertainties are ±0.3 °C on $T_d$ and within 6% of the reported value on $\Delta_d H(T_d)$. The correctness of the use of the two-state N ⇄ D model to describe the denaturation processes is given by the closeness to one of the cooperative unit parameter, CU, given by the calorimetric to van't Hoff enthalpy ratio, $CU = \Delta_d H(T_d)/\Delta_d H(T_d)_{vH}$ [19,20].

The denaturation heat capacity change, $\Delta_d C_p$, couldn't be obtained directly due to the high denaturation temperatures [10]; an indirect method has been used, based on the thermodynamic relationship between $\Delta_d H(T_d)$ and $T_d$: $\Delta_d C_p = \partial \Delta_d H(T_d)/\partial T_d$. To apply this relationship, different experimental conditions can be used, that are proven not to

affect the final $\Delta_dC_p$ value (i.e., pH variation, increasing denaturant concentration, etc.) [21]. An increasing denaturant concentration, but still within the pre-denaturation region, has been used in the present study.

Having the $\Delta_dC_p$ value, it is possible to determine the denaturation Gibbs energy change at each temperature, $\Delta_dG(T)$, and in particular its value at 25 °C, using the Gibbs-Helmholtz equation:

$$\Delta_d G(T) = \Delta_d H(T_d)(1-T/T_d) + \Delta_d C_p[T-T_d-T\ln(T/T_d)]$$

### 2.5. Isothermal titration calorimetry

ITC measurements were performed using a Nano-ITC III (TA instruments, New Castle, DE, USA) at 25 °C. A 35 μM D1 protein solution (ligand-free form) was titrated with a 300 μM GuHCl solution at pH 7.4. Each injection was of 10 μL, with 500 s intervals between the individual injections; the heat variation after each addition is measured with respect to a reference cell filled with buffer. Small heat changes recorded after full saturation, caused by ligand dilution and other nonspecific effects, have been subtracted from the areas of the initial peaks. Data fitting was conducted with the Nano-Analyze software package supplied by the manufacturer. The binding enthalpy change, $\Delta_bH$, is given by the height of the sigmoidal binding curve; the stoichiometry of the process comes from the molar ratio corresponding to the inflexion point; the binding constant, $K_b$, which is the reciprocal of the dissociation constant, is obtained by fitting experimental data to an independent binding model. ITC runs were repeated twice to evaluate the reproducibility of the results.

### 2.6. Protein crystallization, data collection and structure refinement

Crystallization experiments were performed at 293 K on a solution containing both the D1 domain and GuHCl by using hanging-drop vapor diffusion methods. Crystals of the putative adduct were obtained using a protein concentration of 6 mg $mL^{-1}$ and a medium containing 0.2 M NaCl, 0.2 M GuHCl, 0.1 M Bis-Tris (pH 5.5), and 25% (w/v) polyethylene glycol (PEG) 3350.

Diffraction data were collected in-house using a Rigaku Micromax 007 HF generator equipped with a Saturn944 CCD detector at 100 K. The data were collected by flash-cooling in the supercooled $N_2$ gas produced by an Oxford Cryo-system after the addition of 20% ethylene glycol to the harvesting solution.The data set was scaled and merged using the HKL2000 program package [22]. The crystals, which contain two molecules per asymmetric unit, belong to the P1 space group and diffracted at 1.7 Å (Table 1).

The structure of the putative complex was solved by molecular replacement using the program Phaser [23] and the structure of the ligand-free form of D1 (PDB code 6GPD) as starting model. From this solution a reliable model was obtained by the automatic modeling performed with ARP/wARP [24]. The crystallographic refinement of the structure has been carried out using the program REFMAC [25]. Inspection of the putative $GuH^+$ binding site revealed the presence of electron density that could correspond to the ion. In particular, the ion is clearly visible in the pocket of one molecule present in the asymmetric unit (Molecule A) (Fig. S1A), whereas the electron density observed in the other one has been interpreted with a $GuH^+$ ion with a 0.5 occupancy and with an alternative pair of water molecules also with a 0.5 occupancy (Fig. S1B). Water molecules were incorporated into the structure in several rounds of refinements. The final model presents R-factor and R-free values of 0.162 and 0.187, respectively. The stereochemistry of the final model has been checked by using both standard validation protocols (wwPDB validation, https://validate-rcsb-2.wwpdb.org/) and Molprobity [26] and innovative approaches that are based on the evaluation of the conformation-dependent variability of the peptide geometry (http://study.ibb.cnr.it/quiproqua/) [27–30]. As shown in Table 1, the analysis of the final model performed using Molprobity indicates that it is endowed with a good stereochemistry. Indeed, the φ,ψ values of all residues fall in allowed regions of the Ramachandran plot with the vast majority adopting favored conformations (98.4%). Moreover, no bad bonds and Cβ deviations are detected whereas a negligible number of valence bonds presents a distorted geometry. To further evaluate the accuracy of bond and dihedral angles of the final model, the variability of backbone valence angles and of the peptide planarity as a function of the local conformation was checked. As shown in Fig. S2 and Table S1, the variability of these parameters follows the trends detected in highly accurate protein structures [27–29]. The atomic coordinates of the D1-$GuH^+$ complex have been deposited in the PDB with the identification code 6y16.

**Table 1**
Data collection and refinement statistics of the D1-$GuH^+$ complex. Values in parentheses are for the highest resolution shell (1.76–1.70 Å).

| Protein | ArgBP D1-$GuH^+$ |
|---|---|
| X-ray device | Rigaku FR007HF with CCD detector |
| Space group | P1 |
| a, b, c (Å) | 35.45, 45.81, 52.41 |
| α, β, γ (°) | 64.07, 70.33, 90.02 |
| Resolution range (Å) | 50.00–1.70 |
| Wavelength (Å) | 1.54 |
| Average redundancy | 2.7 |
| Unique reflections | 25,777 |
| Completeness (%) | 85.0 (45.9) |
| R merge (%) | 6.6 (25.1) |
| Average I/σ(I) | 20.2 (2.7) |
| Asymmetric unit | dimer |
| R/R-free | 0.162/0.187 |
| No. of residues | 254 |
| No. of ligand molecules | 4 (2 GAI, 2 EDO) |
| No. of water molecules | 263 |
| Mean B values ($Å^2$) | |
| Protein atoms | 19.8 |
| Ligand atoms | 20.0 |
| Water atoms | 28.0 |
| R.m.s. bonds (Å) | 0.008 |
| R.m.s. angles (°) | 1.623 |
| MolProbity statistics | |
| MolProbity score | 1.56 |
| Clashscore, all atoms: | 6.46 |
| Ramachandran allowed | 254/254 (100%) |
| Ramachandran favored | 250/254 (98.4%) |
| Ramachandran outliers | 0/254 (0%) |
| Favored rotamers | 206/216 (94.1%) |
| Poor rotamers | 4/216 (2.3%) |
| Cβ deviation >0.25 Å | 0/232 (0%) |
| Bad bonds | 0/2010 (0%) |
| Bad angles | 5/2715 (0.18%) |

### 2.7. Molecular dynamics: models and protocol

Two independent molecular dynamics (MD) simulations were performed on the crystallographic model of the D1 domain generated in the present study. In particular, we performed the simulation on the complex with $GuH^+$ and, for comparative purposes, on the ligand-free form of the domain that was obtained by removing the ion from the binding pocket. The three-dimensional structure of molecule A was used as starting model in the simulations. MD simulations were carried out using the version 2018.3 of GROMACS package and the OPLS-AA force field [31]. The protein models were solvated with water molecules (the TIP4P model was used) in triclinic boxes imposing a minimum distance of 10 Å between the proteins and the box. The systems were neutralized adding sodium counterions. Electrostatic interactions were treated by means of the particle-mesh Ewald (PME) method with a grid spacing of 1.6 Å [32], together with a 10 Å cut-off for the Lennard-Jones (LJ) interactions. The LINCS algorithm was used for constraining bond lengths [33]. Systems were first energy minimized using steepest descent and then equilibrated in two steps. In the first

phase, the temperature of the systems was stabilized at 300 K for 500 ps (NVT). Equilibration of pressure at 1 atm was then conducted for other 500 ps (NpT). The Velocity Rescaling and Parrinello-Rahman algorithms were applied for temperature and pressure control, respectively [34,35]. The production runs were carried out for 200 ns for each system with a time step of 2 fs. The convergence of the production runs has been checked by calculating the root mean square inner product (RMSIP) between the two halves of the equilibrated trajectory considering the motion of the protein $C^{\alpha}$ atoms along the first 10 eigenvectors [36,37]. In detail, the last 100 ns of each trajectory was divided in two halves (100–150 ns and 150–200 ns). The high values of the RMSIP (0.81 for D1 and 0.83 for D1-$GuH^+$) between these two trajectory portions suggest that a satisfactory level of convergence is reached. Structural analyses of trajectory structures were performed using GROMACS routines and the program VMD [28,29,38].

### 2.8. Survey of guanidium-containing structures in the Protein Data Bank

The initial search for the protein structures containing the $GuH^+$ ion was performed by interrogating the entire Protein Data Bank (release of April 2020) using as a query the three letter code GAI that identifies this ion in PDB files. The server identified 91 entries where GAI is present as a standalone ligand. Of these, 10 entries were excluded as they correspond to RNA-$GuH^+$ complexes. The remaining 82 $GuH^+$ ion containing protein structures (including the structure of D1-$GuH^+$ here reported; PDB entry 6y16) were initially analyzed in terms of the number of $GuH^+$ present in the asymmetric unit (Fig. S3 and Table S2).

Inspection of Table S2 highlights that some entries refer to the same protein molecule. To avoid redundancy, when the same protein type was reported in multiple PDB entries, we selected the one containing the highest number of $GuH^+$ ions in the asymmetric unit (A.U.). In the case of entries containing the same number of bound ions, the structure solved at the highest resolution was considered (Table S3). In the case of the Arginase protein, two distinct entries (3cev and 2ef5) have been considered in the analysis since the two proteins are derived from different species (*B. caldevelox* and *T. thermophilus*; 53.9% sequence identity). After this selection, we ended up with a total of 167 $GuH^+$ ions bound (see $GuH^+$ in A.U. of Table S2). The interactions established by all these $GuH^+$ ions with the protein residues (and cofactors/ions) were computed using the LigPlus [39] server together with manual inspection of the PDB structures. LigPlus identifies the protein residues or cofactor/ions interacting with ligands using the following criteria: (a) a distance within 3.35 Å for H-bonding and (b) a distance within 3.90 Å for the interactions with the aromatic/aliphatic groups. Since LigPlus does not consider interactions of the ligand with (i) water molecules and (ii) symmetry-related mates in the crystalline state, we individually inspected all these entries using COOT and annoted also this type of interactions.

As shown in Table S3, in 15 (entries underlined in the table) out of the 37 entries selected for our analysis the asymmetric unit contains more copies of the biological assembly (B.A.). In the latter cases, the same enviroment of the $GuH^+$ ion is frequently detected in the different B.A. present in the same A.U. When this happens, to avoid redundancy, we selected only one representative example of the repetitive binding site within different B.A. present in the same entry. After this selection, we ended up with a total of 117 protein-bound $GuH^+$ ions (see the column $GuH^+$ in B.A. of Table S3). Additionally, for multimeric proteins a similar/identical enviroment of the $GuH^+$ ion is observed for the different chains of the oligomer and, again, to avoid redundancy, we selected only one representative example of the repetitive binding site within protein oligomers. After this further selection, we ended up with a total of 92 independent $GuH^+$ ions bound (see independent $GuH^+$ in Table S3).

## 3. Results

### 3.1. Chemical denaturation

As in other substrate binding proteins, in TmArgBP the functionality of the protein is assured by an intricate mutual rearrangement of its two constitutive D1 and D2 domains (Venus fly-trap mechanism [40]). We here investigated the stability against GuHCl of these domains in their

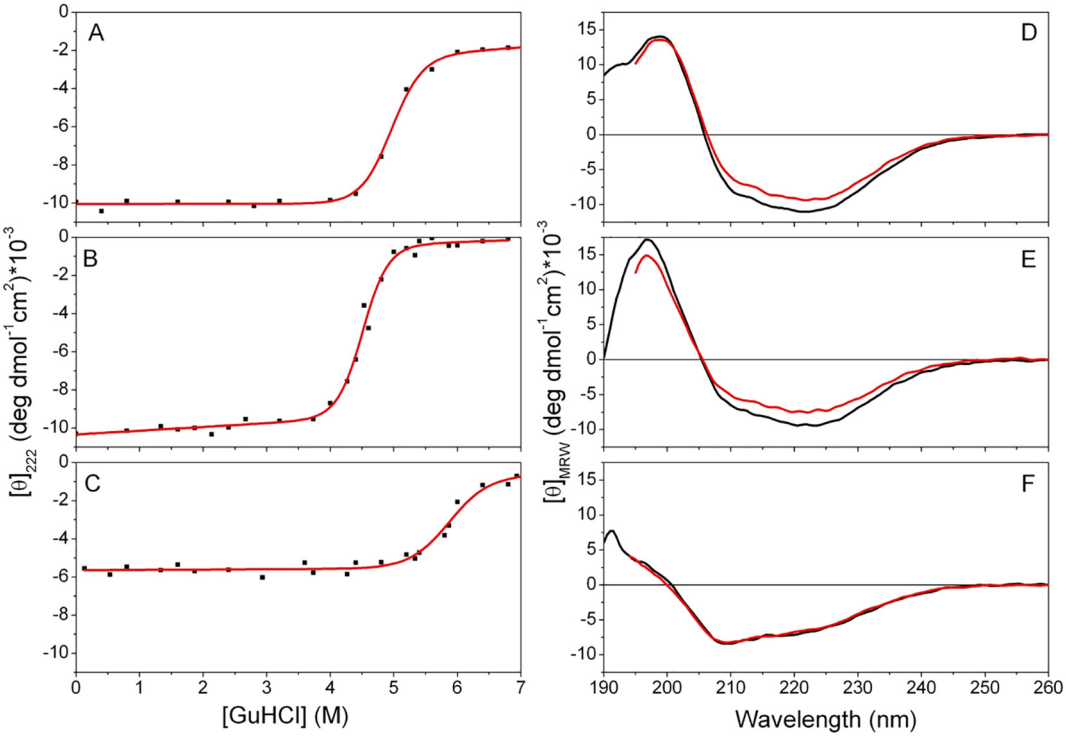


**Fig. 1.** Left panels: chemical denaturation curves from CD measurements of A) $TmArgBP^{20-233}$, B) D1 domain and C) D2 domain. Right panels: reversiblity check of D) $TmArgBP^{20-233}$, E) D1 domain and F) D2 domain denaturation processes; black lines indicate native spectra, red lines represent the spectra of the denatured samples after GuHCl removal.

**Table 2**
Parameters from chemical denaturation experiments on TmArgBP$^{20–233}$, D1 and D2, obtained by fitting the corresponding plots of $[\theta]_{222}$ versus [GuHCl] by the nonlinear least squares method described in Section 2.3. The value of $R^2$ is 0.99 for each curve.

| Sample | $C_{1/2}$ (M) | $m$ (kJ mol$^{-1}$ M$^{-1}$) | $\Delta_dG(H_2O)$ (kJ mol$^{-1}$) |
|---|---|---|---|
| *Tm*ArgBP$^{20–233}$ | 5.0 | 11 ± 1 | 54 ± 8 |
| D1 | 4.5 | 12 ± 1 | 55 ± 8 |
| D2 | 5.9 | 8 ± 1 | 46 ± 7 |

isolated states and compared it to the one exhibited by the monomeric functional form TmArgBP$^{20–233}$. All three proteins show a high stability towards the denaturing action of GuHCl: the values of the denaturant concentration at half of the transition, $C_{1/2}$, are always larger than 4 M (see Fig. 1 and Table 2). The GuHCl-induced denaturation curves, obtained by recording the CD signal at 222 nm, have a clear sigmoidal shape indicative of a cooperative process. The latter proves to be reversible: the far-UV CD spectra of the three proteins, after denaturation and suitable removal of GuHCl, prove to be close to those of fresh protein samples (see Fig. 1). Denaturation curves, analyzed by means of the LEM model, have given the values of the *m* parameter and denaturation Gibbs energy change at zero denaturant concentration, $\Delta_dG(H_2O)$, listed in Table 2. The conformational stability of the two domains, D1 and D2, is similar to that of TmArgBP$^{20–233}$: the three $\Delta_dG(H_2O)$ values are all around 50 kJ mol$^{-1}$. The *m* parameter values (i.e., 11, 12 and 8 kJ mol$^{-1}$ M$^{-1}$ for TmArgBP$^{20–233}$, D1 and D2, respectively) are compatible with cooperative processes. These findings are also in line with the functional role of these domains. Indeed, as they are structurally independent when the substrate is released, they must be intrinsically endowed with a remarkable stability. Nevertheless, the $C_{1/2}$ values suggest a greater compactness and stability of D2 ($[GuHCl]_{1/2} = 5.9$ M) compared to D1 ($[GuHCl]_{1/2} = 4.5$ M), which hosts the binding site for arginine and is probably more flexible. In this scenario, the intermediate stability exhibited by TmArgBP$^{20–233}$ is not surprising.

### 3.2. DSC measurements

The stability against temperature of TmArgBP$^{20–233}$, D1 and D2 in aqueous buffer solution has already been investigated, and the temperature-induced denaturation proved to be reversible for all the three proteins [10]. The experimental values of $T_d$ and $\Delta_dH(T_d)$, in the absence and in the presence of GuHCl at concentrations ranging from 0.2 to 2.5 M, are listed in Table 3; the corresponding DSC traces are shown in Fig. 2. On increasing the GuHCl concentration, the $T_d$ and $\Delta_dH(T_d)$ values decrease significantly, as expected for the denaturing action of the guanidinium ion. The process is reversible, and the CU value is close to one in all the cases, indicating that the temperature-induced denaturation of the three proteins can be described as a reversible two-state transition.

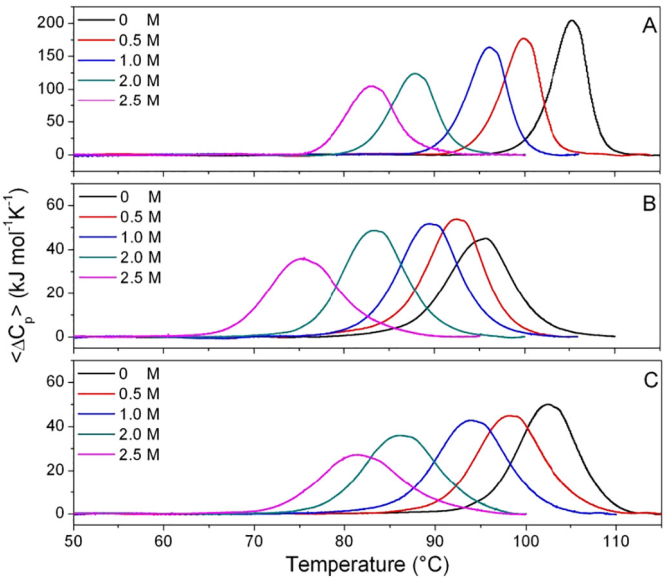


**Fig. 2.** DSC curves of A) TmArgBP$^{20–233}$, B) D1 and C) D2 in the absence and in the presence of GuHCl at the concentrations indicated in the boxes.

By plotting the $\Delta_dH(T_d)$ values versus the $T_d$ ones at 0 M, 0.5 M, 1.0 M, 2.0 M and 2.5 M GuHCl for all the three proteins (an exception is D1, for which the point at 0.2 M GuHCl is considered instead of the point in the absence of denaturant, because of an unusual behavior that will be illustrated in the next paragraph), it has been possible to arrive at reliable $\Delta_dC_p$ estimates by performing a linear least-square regression (see Table 3). The value of $\Delta_dC_p$ derived experimentally for D2, 6.8 ± 0.7 kJ mol$^{-1}$ K$^{-1}$, is greater than the one for D1, 4.9 ± 0.5 kJ mol$^{-1}$ K$^{-1}$. This is in line with the measured $\Delta_dH(T_d)$ values: in aqueous buffer solution the denaturation enthalpy change is greater for D2 than for D1, suggesting that more and/or stronger interactions are broken in the former upon denaturation (see Table 3). The $\Delta_dG$ (25 °C) values calculated using the obtained $\Delta_dC_p$ estimates in the Gibbs-Helmholtz equation, are similar to the corresponding $\Delta_dG(H_2O)$

**Table 3**
DSC data of TmArgBP$^{20–233}$, D1 and D2 in the absence and in the presence of GuHCl and the derived thermodynamic parameters $\Delta_dC_p$ and $\Delta_dG$(25 °C), obtained as described in Section 2.4. The reported $T_d$ and $\Delta_dH(T_d)$ values are the average of three measurements. The uncertainties are 0.3 °C on $T_d$, 6% on $\Delta_dH(T_d)$, 10% on $\Delta_dC_p$ and about 30% on $\Delta_dG$(25 °C).

| Sample | [GuHCl] (M) | $T_d$ (°C) | $\Delta_dH(T_d)$ (kJ mol$^{-1}$) | CU | $\Delta_dC_p$ (kJ mol$^{-1}$ K$^{-1}$) | $\Delta_dG$(25 °C) (kJ mol$^{-1}$) |
|---|---|---|---|---|---|---|
| TmArgBP$^{20–233}$ | – | 105.3 | 1000 | 1.0 | 17 | 56 |
| | 0.5 | 99.8 | 980 | 1.1 | | |
| | 1.0 | 96.0 | 920 | 1.1 | | |
| | 2.0 | 87.8 | 800 | 1.0 | | |
| | 2.5 | 83.0 | 660 | 1.0 | | |
| D1 | – | 95.5 | 450 | 0.98 | 5 | 50 |
| | 0.2 | 94.7 | 480 | 0.99 | | |
| | 0.5 | 92.4 | 460 | 0.98 | | |
| | 1.0 | 89.5 | 460 | 0.98 | | |
| | 2.0 | 83.3 | 430 | 0.96 | | |
| | 2.5 | 75.6 | 380 | 0.97 | | |
| D2 | – | 102.6 | 470 | 0.96 | 7 | 36 |
| | 0.2 | 100.8 | 450 | 0.96 | | |
| | 0.5 | 98.2 | 440 | 0.96 | | |
| | 1.0 | 94.0 | 430 | 0.98 | | |
| | 2.0 | 86.2 | 370 | 0.95 | | |
| | 2.5 | 81.5 | 320 | 0.97 | | |

values obtained from the LEM analysis of GuHCl-induced denaturation curves. D2 appears to be less stable using DSC data, but it should be remembered that the $\Delta_dG(25\ °C)$ values are affected by a high error, because their calculation requires extrapolation over an extended temperature range; so a small error in $\Delta_dC_p$ causes a significant change in the final $\Delta_dG(25\ °C)$ value. The normalization per residue of the $\Delta_dG$ (25 °C) values indicates a greater stabilization in the case of the D1 and D2 domains than for the monomer (about 400 J $mol^{-1}$ $res^{-1}$ for the domains versus 260 J $mol^{-1}$ $res^{-1}$ for $TmArgBP^{20–233}$).

### 3.3. Binding of guanidinium ion to D1

DSC measurements of D1 in the presence of GuHCl at low concentrations gave an unusual behavior (see Fig. 3). In the presence of 0.2 M GuHCl, D1 exhibits $\Delta_dH(T_d) = 480$ kJ $mol^{-1}$, higher than the value in the aqueous buffer solution alone, which corresponds to 450 kJ $mol^{-1}$; the denaturation temperature decreases slightly from 95.5 ± 0.3 °C to 94.7 ± 0.3 °C (see Table 3). At low concentration, then, the guanidinium ion does not act as a denaturant for D1, suggesting that different mechanisms from the usual ones (e. g., [41,42]) play a role. To gain perspective, it has to be noted that, in the case of D2, the $T_d$ value decreases from 102.6 ± 0.3 °C for the sample in aqueous buffer solution alone to 100.8 ± 0.3 °C for the sample in 0.2 M GuHCl, and $\Delta_dH(T_d)$ decreases from 470 to 450 kJ $mol^{-1}$. This confirms that GuHCl acts as a denaturant for D2 also at low concentrations. The different effects that GuHCl has on the two domains at low concentrations may be due to the different role that D1 and D2 have in the binding of arginine whose guanidinium group closely resembles the $GuH^+$ ion. Although both domains cooperate into the binding of the substrate in the wild-type protein [8], only the D1 domain is able to bind arginine in its isolated state [10]. This observation suggests the possibility that the $GuH^+$ ion may be able to bind the D1 pocket, despite the lack of the other anchoring groups that facilitate arginine binding, and to establish favorable interactions that stabilize the domain.

To evaluate and possibly corroborate this hypothesis, we initially performed ITC measurements (see Fig. 4). These data clearly indicate that the guanidinium ion interacts with D1. On the other hand, no binding has been detected by ITC measurements in the case of D2. Table 4 reports the values of n, $K_b$, and $\Delta_bH$ obtained from the titration of D1 with GuHCl, in comparison to those obtained from the titration of D1 with arginine (taken from [10]). The stoichiometry of the reaction is 1, while the binding constant $K_b = 2.9 \cdot 10^5$ $M^{-1}$, about one order of magnitude lower than that for arginine ($3.6 \cdot 10^6$ $M^{-1}$). This finding is not surprising as the aminoacid forms with the protein a larger network of interactions, both polar/electrostatic and hydrophobic, than that of $GuH^+$.

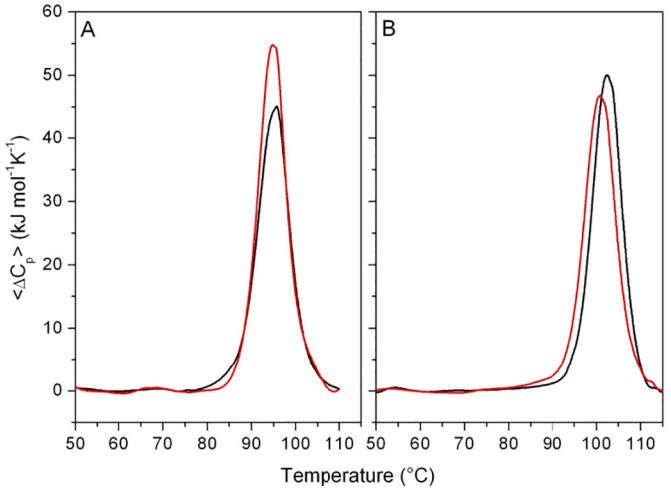


**Fig. 3.** DSC profiles of A) D1 and B) D2 in PBS (black lines) and 0.2 M GuHCl (red lines).

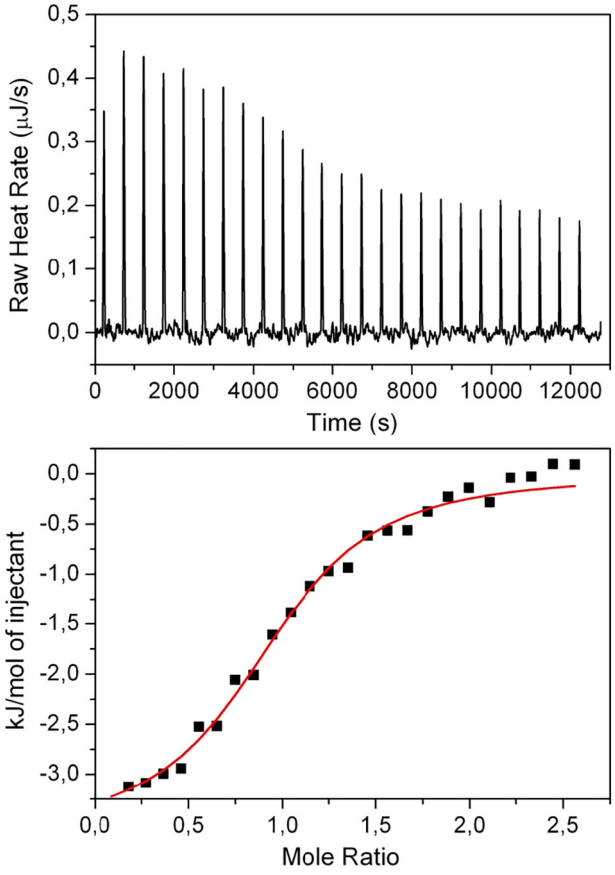


**Fig. 4.** Titration of apo-D1 with GuHCl followed by means of ITC.

The binding enthalpy change is $\Delta_bH = -3.6 \pm 0.3$ kJ $mol^{-1}$ for $GuH^+$, a value much smaller in magnitude than that for arginine binding, $-54 \pm 2$ kJ $mol^{-1}$ [10]. This finding indicates an entropy-driven binding process in the case of $GuH^+$, in contrast with the enthalpy-driven binding process of arginine.

### 3.4. Structure and dynamics of the D1-$GuH^+$ complex

To gain further insight into the possible interaction that D1 can establish with $GuH^+$, we grew crystals of the domain in the presence of 0.2 M GuHCl, a concentration at which the guanidinium ion does not act as a denaturant. The crystal structure of the complex between D1 and $GuH^+$ has been solved to 1.7 Å resolution (the refinement statistics are listed in Table 1). The two copies of the domain present in the asymmetric unit of the crystal of the D1-$GuH^+$ complex show a very similar structure, as indicated by the low value (0.234 Å) of the root mean square deviation (RMSD) computed on the $C^\alpha$ atoms of the two chains. Small RMSD values (Table S4) are detected when the D1 domain of the D1-$GuH^+$ structure is compared to the previously reported D1 structures (ligand-free and arginine-bound forms). Larger RMSD values (Table S4) are found when the present D1 domain is compared to structures where D1 is embodied in larger contexts (monomeric and dimeric structures of TmArgBP). The inspection of the D1 substrate binding pocket showed the presence of electron density that was interpreted as a $GuH^+$ ion in molecule A, and as a mixture of waters and $GuH^+$ ion in molecule B (Fig. S1).

The analysis of the crystallographic structure indicates that the $GuH^+$ ion is anchored at the arginine binding site of the protein. In particular, it is located in the portion of the pocket that binds the guanidinium group of the arginine, the natural ligand of the protein (Fig. 5A and B). The tight anchoring of the ion is due to different types of interactions (Fig. 5B and C). Of particular relevance is the role played

**Table 4**
ITC data from the titration of ligand-free D1 domain with GuHCl compared to the values from its titration with arginine [10].

| Injectant | n | $\Delta_bH$ (kJ $mol^{-1}$) | $K_b$ ($M^{-1}$) |
|---|---|---|---|
| GuHCl | 1 | −3.6 ± 0.3 | $2.9 \cdot 10^5$ |
| Arg (from [10]) | 1 | −54 ± 2 | $3.6 \cdot 10^6$ |

by the aromatic rings of Phe19 and Phe57 that sandwich the $GuH^+$ ion through cation-π interactions, as recently seen in other adducts between the $GuH^+$ ion and lysozyme [43]. The ion is also anchored by polar (carbonyl oxygen of Ser74 and Ser16 and the Oγ atom of Ser74) and charged (side chain of Asp18 and Glu23) groups. On the basis of the extensive network of interactions established by the ion in the substrate binding pocket of the domain, it is not surprising the effect that it has on the D1 stability.

In order to gain a dynamic view of the intricate interaction network that characterizes the $GuH^+$ anchoring by D1, we performed a MD simulation on the complex. We also carried out a simulation on the $GuH^+$-free form of D1 for comparative purposes. The stability of the domain in the MD simulations was initially evaluated by analyzing the time evolution of some structural indicators as the root-mean square deviation (RMSD) of trajectory structures against the starting X-ray crystallographic model and the gyration radius (Fig. S4). The monitoring of these parameters indicate that in both cases the systems reached a satisfactory level of stability in the simulation timescale. Inspection of the RMSD variability highlighted a *plateau* region in the 70–200 ns timescale interval.

Analysis of the specific interactions that stabilize the complex in the trajectory structures indicates that those identified in the crystalline state are rather preserved throughout the simulation, although a temporal variability can be detected. In particular, the inspection of the cation-π interactions indicates that the side chains of both Phe19 and Phe57 remain in proximity of the $GuH^+$ ion throughout the simulation (Fig. 6A and B). Analysis of the polar interactions that stabilize the binding was conducted by separately considering electrostatic (Figs. 6C and S5) and H-bonding (Figs. 6D and S6) interactions. Elecrostatic interactions are rather well preserved in the trajectory structures. However, analysis of the distance evolution points out that the interacting oxygen atom of the aspartic/glutamic side chains frequently changes as a consequence of the flipping motion of terminal carboxylate groups. The distances reported in Fig. S5 suggest that also the nitrogen atoms of $GuH^+$ can swap, and that the ligand moves within the binding pocket. A similar picture emerges on looking at the H-bonds formed within the binding pocket: the contacts are dynamically preserved thoughout the simulation (Figs. 6D and S6). The only significant difference with the pattern observed in the crystal state is the interaction of the $GuH^+$ ion with Ser16. While in the crystallographic structure $GuH^+$ forms a H-bond with the oxygen atom of Ser16 backbone, in the trajectory structures this interaction preferably involves the $O^{\gamma}$ atom of its side chain.

Finally, we evaluated the impact of the $GuH^+$ binding on the global and local flexibility of D1 domain. In particular, we compared the root mean square fluctuations (RMSF) values obtained from the simulations carried out on the $GuH^+$-free and bound state of the domain. As shown in Fig. S7, in both simulations the most rigid regions correspond, as expected, to the secondary structure elements of the protein. Notably, a comparative analysis of the RMSF values indicates that the regions deputed to the $GuH^+$ anchoring become more rigid upon its binding (Fig. 7).

### 3.5. Guanidium binding to proteins: a comphensive analysis of PDB

The elevated number of diversified interactions that stabilize the complex between D1 and $GuH^+$ promped us to check whether this is a peculiar or common condition for guanidinium binding to proteins. To this aim, we interrogated the entire Protein Data Bank (release of April 2020) looking for protein-$GuH^+$ complexes. As detailed in the Materials and methods section, we found 82 PDB entries containing such complexes. These entries correspond to 37 distinct proteins (Table S3). After a detailed curation of these entries to avoid redundancy (see the Materials and methods section), we identified a total of 92 independent $GuH^+$ ions bound (see independent $GuH^+$ in Table S3). All of these binding sites were inspected by using LigPlus and molecular graphics to unravel and classify the interactions that favor the ion binding to proteins. In particular, the following interactions were considered: (a) H-bonds (with main chain or side chain protein residues), (b) hydrophobic (aliphatic or aromatic) interactions, (c) salt bridges, (d) contacts between $GuH^+$-Arg and $GuH^+$-$GuH^+$ groups, and (e) interactions with cofactors and solvent. In Table 5, the frequency of these types of interactions is reported as the percentage of $GuH^+$ binding sites displaying them.

As a general observation, we found that most of the $GuH^+$ ions make a remarkable number of diversified interactions with their protein partner (Table 5 and Fig. S8). Frequent contacts include H-bonds, electrostatic and hydrophobic interactions. Some representative examples are reported in Fig. 8. Of particular relevance is the finding that hydrophobic contacts are observed in almost all binding sites. These include interactions with both aliphatic (a total of 172 contacts) and aromatic (a total of 44 contacts) groups. The analysis of the interacting geometry between the ion and the aromatic groups indicates that these are stabilized by either stacking (32%) or non parallel interactions (68%) (Fig. 8B and C). A significant number of $GuH^+$ ions interacts also with other $GuH^+$ ions or with the guanidinium group of the Arg side chain for a total of 25 contacts (18 with the guanidinium group of Arg side chains).

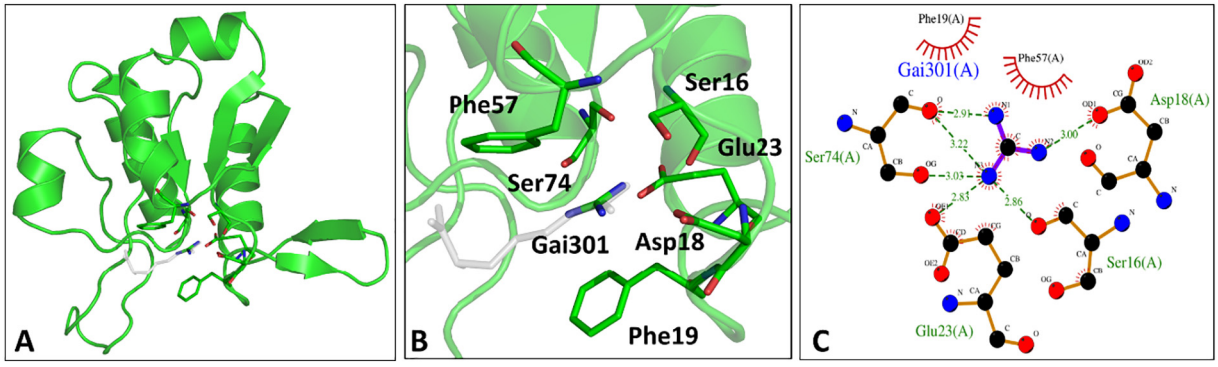


**Fig. 5.** A) Cartoon representation of the crystal structure of the D1 domain in complex with $GuH^+$; B) Zoom view of the binding site. The residues of the D1 pocket that interact with $GuH^+$ ion are represented as sticks. For comparative purposes, the arginine amino acid (white) as bound in the D1-arginine complex (PDB entry 6GPC) is also shown; C) Network of the interactions established by $GuH^+$ with D1 residues obtained with LigPlus [39].

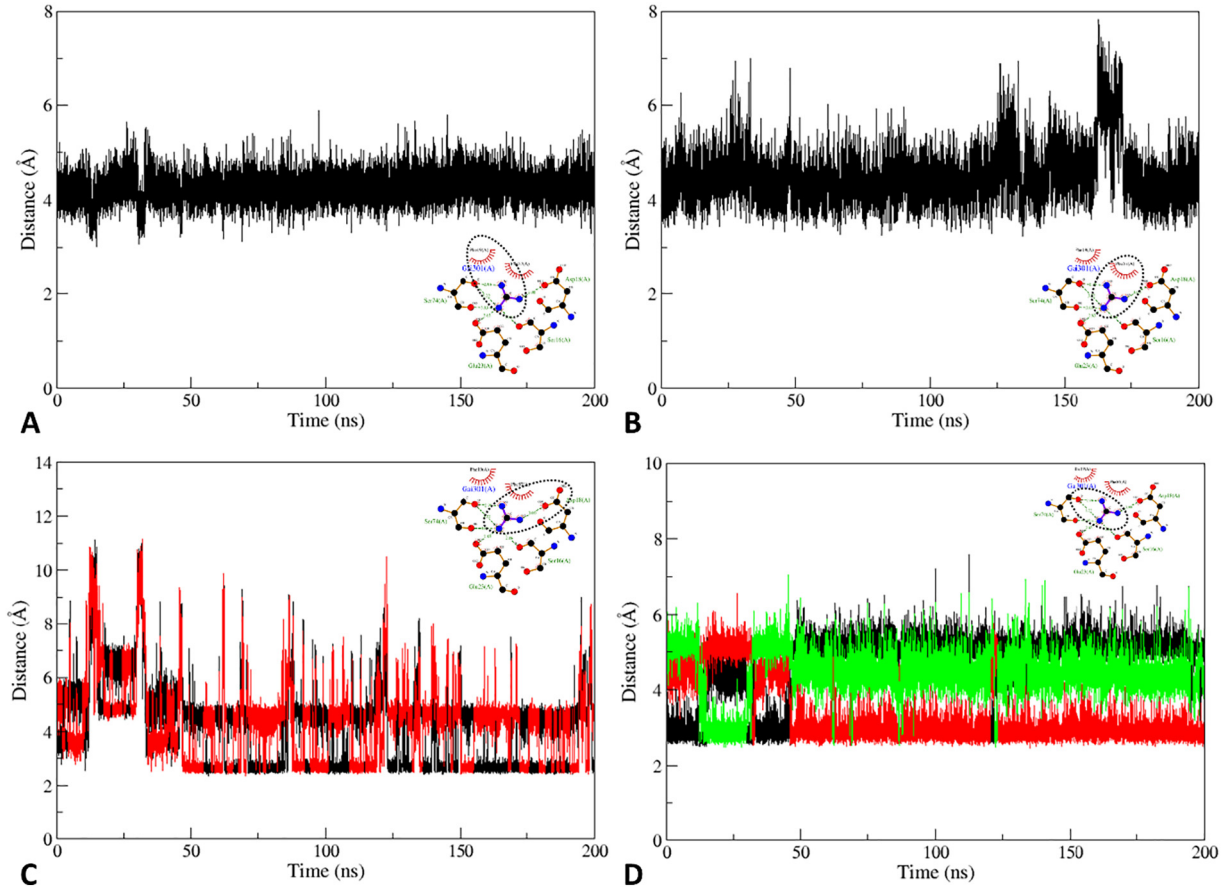


**Fig. 6.** Representative examples of hydrophobic, electrostatic and H-bonding interactions between $GuH^+$ and protein residues in the simulation of D1-$GuH^+$: A) $GuH^{+C}$-$Phe19^{C\gamma}$, B) $GuH^{+C}$-$Phe59^{C\gamma}$, C) $GuH^{+N3}$-$Asp18^{O\delta1}$ (black) and $GuH^{+N3}$-$Asp18^{O\delta2}$ (red), and D) $Ser74^{O}$ to $GuH^{+N1}$ (black), $GuH^{+N2}$ (red), $GuH^{+N3}$ (green) distances. The scheme of the interacting groups is reported as inset in each plot.

A significant portion of them presents a stacking geometry between the $GuH^+$ groups. It is important to note that, in these cases, the surrounding is frequently rich in negatively charged residues (Asp or Glu) that render feasible this electrostatically disfavored interaction.

A remarkable number of $GuH^+$ ions are located at the protein-protein interface. We identified 39 out of the 92 $GuH^+$ ions (42%) forming interactions with symmetry related molecules. Additionally, 10 out of the 92 $GuH^+$ ions (11%) are located at the protein-protein interface between chains within the oligomeric assembly, whereas only 4 $GuH^+$ ions (4%) are located at the interface joining different protein chains that are present in the asymmetric unit. Finally, although many of these ions interact with water molecules, almost one third of them do not interact with solvent, suggesting that they are buried either inside the protein or at water-inaccessible protein-protein interfaces.

## 4. Discussion

The conformational stability of $TmArgBP^{20–233}$ and its D1 and D2 domains towards GuHCl has been investigated using a combined calorimetric and spectroscopic approach. The obtained denaturation Gibbs

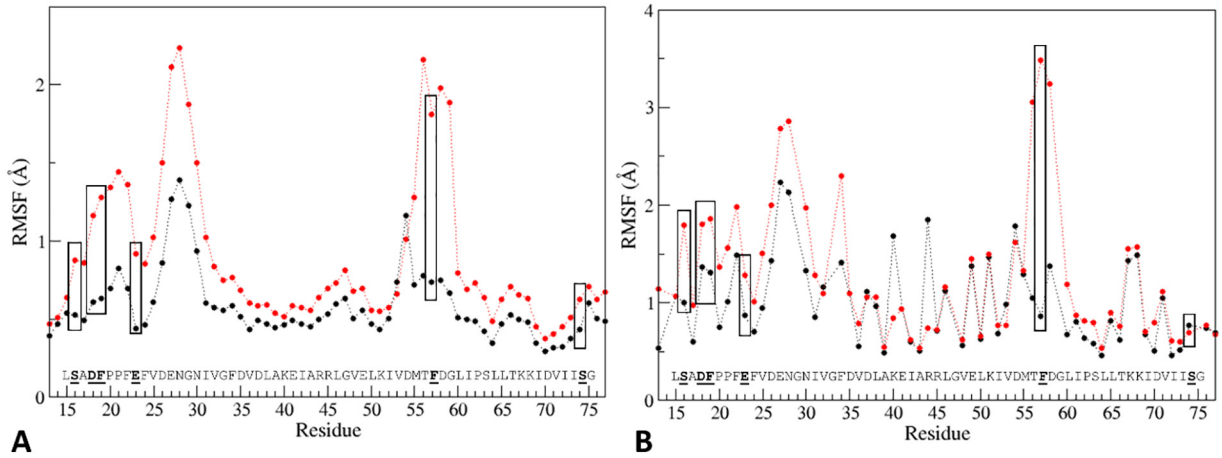


**Fig. 7.** RMSF values computed on D1 $C^{\alpha}$ (A) or side chain (B) atoms in the 70–200 ns region of the MD trajectories in the simulations of D1 (black) and D1-$GuH^+$ (red). The protein region containing the residues that interact with the $GuH^+$ ion is shown. Residues Ser16, Asp18, Phe19, Glu23, Phe57, and Ser74 are highlighted.

**Table 5**
The frequency of interactions established by $GuH^+$ ions in our ensemble of protein structures is reported as the percentage of $GuH^+$ binding sites displaying them.

| Type of interaction | Percentage (%) |
|---|---|
| H-bond | 58.7 |
| H-bond with main chain | 48.9 |
| H-bond with side chain | 21.7 |
| Salt bridge | 42.4 |
| Hydrophobic | 96.7 |
| Aliphatic hydrophobic | 85.9 |
| Aromatic hydrophobic | 38.0 |
| Salt Bridge with cofactor | 6.5 |
| Hydrophobic with cofactor | 3.3 |
| Interaction with ion/metal | 1.1 |
| $GuH^+$-Arg guanidinium group | 17.4 |
| $GuH^+$-$GuH^+$ | 6.5 |
| H-bond with water | 70.7 |

energy values suggest a similar stability of about 50 kJ $mol^{-1}$ at room temperature for the three forms under study. This result gives a different scenario from the previously publicated one [10]. It can be rationalized considering that the lower stability may be compensated by a greater structural flexibility, as it was already proposed for the thermal stabilities of the ligand-free form and the bound form of $TmArgBP^{20–233}$ [15].

The second interesting result is the interaction of $GuH^+$ with D1: an unexpected increase in $\Delta_dH(T_d)$ was noted in thermal denaturation of D1 in the presence of low concentrations of GuHCl. It was hypothesized an interaction between this protein, which hosts the binding site for arginine, and the $GuH^+$ ion, which resembles arginine terminal moiety. ITC measurements and the crystal structure of the D1-$GuH^+$ complex support this hypothesis. The $GuH^+$ ion in the complex forms the same interactions as the arginine terminal moiety; the binding affinity is one order of magnitude lower, but the dissociation constant is still in the micromolar range.

Analysis of the interactions that contribute to the tight anchoring of the $GuH^+$ ion to D1 shows that different protein groups participate to the binding. In the complex, $GuH^+$ makes seven different contacts that include H-bonds (involving both main chain and side chain atoms), salt bridges, and hydrophobic interactions (Fig. 5). The ability of D1 to establish multiple and diversified interactions with the $GuH^+$

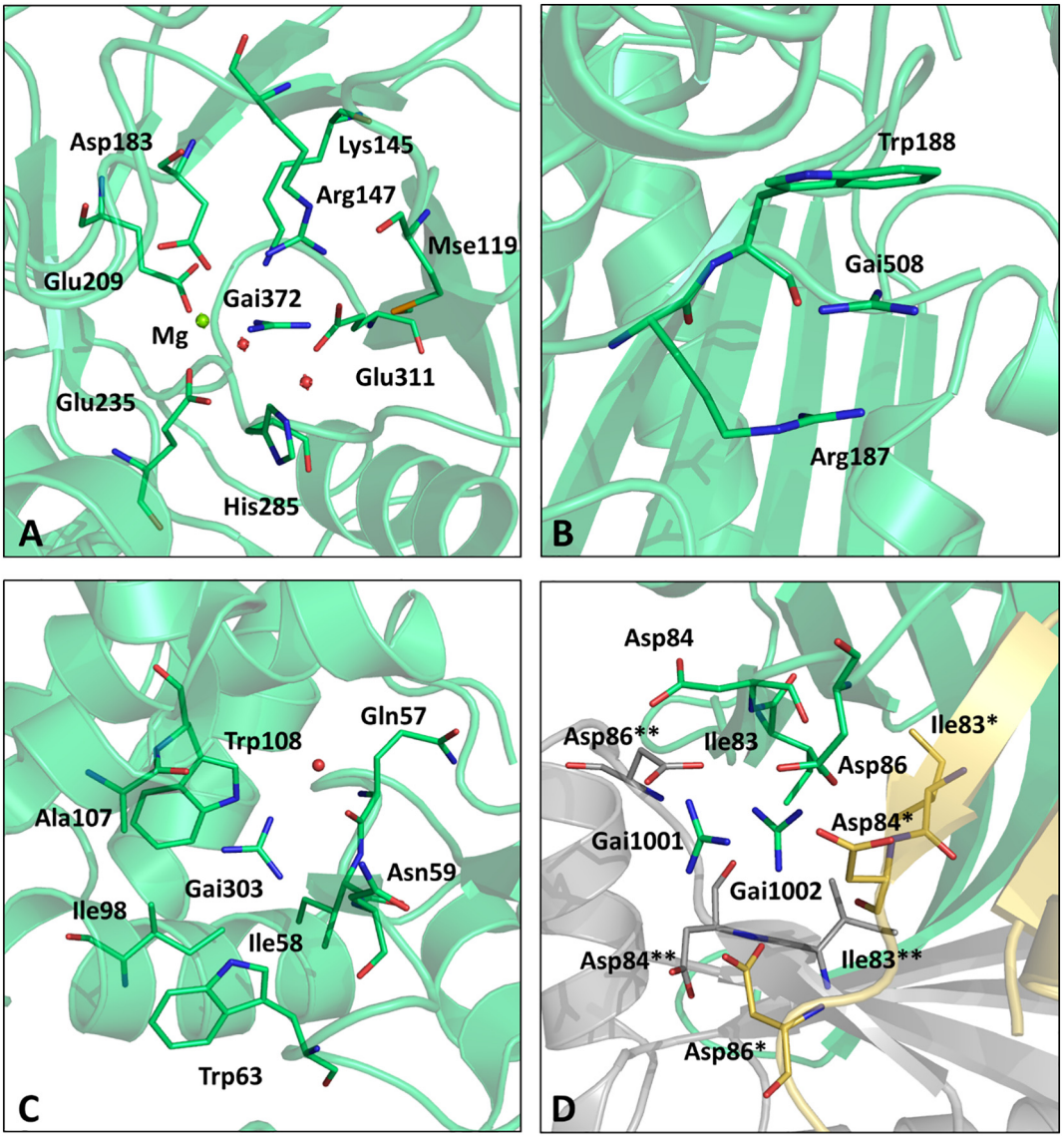


**Fig. 8.** Representative examples of the different types of interactions established by $GuH^+$ in protein structures: A) network of electrostatic, hydrophobic, H-bonding interactions (PDB entry 3u4f, chain C); B) example of aromatic hydrophobic and $GuH^+$-Arg interactions (PDB entry 2ddz, chain E); C) network of hydrophobic interactions (PDB entry 6a4q, chain A); D) $GuH^+$-$GuH^+$ interaction (PDB entry 1umj, chain A). Residues containing at least one polar atom within 3.35 Å and/or one apolar atom within 3.9 Å from the ion are reported. In panel D, the residues of the two symmetry-related mates that cooperates to the $GuH^+$ anchoring are denoted with one or two stars.

ion could be due to the fact that its binding pocket has evolutionarily been designed to anchor the $GuH^+$ group. To discern whether the situation detected in the D1-$GuH^+$ complex was a special or common one, we did a survey of the entire PDB. The annotation and classification of the interactions that $GuH^+$ makes with proteins indicate that the guanidinium ion has a general propensity to make numerous and varied contacts. A significant number of $GuH^+$ ions make interactions with water molecules, aliphatic and aromatic hydrophobic groups, polar atoms, negatively charged residues and even posivitively charged groups (Arg side chains and other $GuH^+$ ions). Although the propensity of this ion to make contacts with different chemical groups of the polypeptide chain has been extensively investigated [43–48], its ability to simultaneously make many different contacts should be a fundamental factor for its denaturing action.

To provide a rationale for the denaturing action of GuHCl, it is useful to look at experimental data on the transfer from water to 4.9 M GuHCl of simple hydrocarbons, at 25 °C and atmospheric pressure [49]. The reported Gibbs energy changes, referring to the transfer from a fixed position in water to a fixed position in 4.9 M GuHCl, are: $\Delta G(\text{in kJ mol}^{-1}) =$ 1.0 for methane, 0.5 for ethane, −0.1 for propane, −0.7 for n-butane, and −1.1 for neopentane. These ΔG values indicate that the process is not thermodynamically favored for small hydrocarbons, but becomes favored for larger ones [49,50]. In addition, the ΔG value for toluene is larger in magnitude than that for neopentane, $\Delta G(\text{in kJ mol}^{-1}) =$ −1.8 versus −1.1 [49,50]. This finding suggests that: (a) the aromatic hydrocarbon is slightly more soluble in 4.9 M GuHCl than an aliphatic hydrocarbon of similar size; (b) the occurrence of cation-π interactions [51] among $GuH^+$ ion and toluene ring has an effect on solubility. This is supported by the finding that $\Delta G = -0.6$ kJ mol$^{-1}$ for the transfer of benzene from water to 5 M GuHCl at 20 °C [52]. On the other hand, the transfer of *N*-acetyl-tryptophanamide from water to 5 M GuHCl at 25 °C has $\Delta G = -3.7$ kJ mol$^{-1}$ [53], indicating that the presence of two peptide groups attached to the indole aromatic ring increases solubility for the establishment of favorable interactions with the $GuH^+$ ion. These experimental thermodynamic data confirm the ability of the guanidinium ion to make favorable interactions with both polar and nonpolar moieties emerged from the analysis of protein crystal structures, and provide a molecular rationalization of its denaturing action.

In conclusion, the study of the conformational stability against GuHCl of the D1 and D2 domains of the monomeric form of TmArgBP has suggested the formation of a complex between D1 and the $GuH^+$ ion. This has been verified by means of ITC measurements and by solving the structure of the D1-$GuH^+$ complex. The multiple and diversified interactions in which $GuH^+$ is engaged in the complex prompted us to verify their commonality in all the protein- $GuH^+$ complexes existing in the PDB. The ability of the guanidinium ion to form multiple and diversified attractive interactions emerges as a peculiar feature of the $GuH^+$ ion, holding not only in protein crystal structures, but also in aqueous solutions. This combined study gives a general rationalization of the $GuH^+$ denaturing action towards the folded state of globular proteins.

## Acknowledgement

The work is supported by funds from the University of Sannio, FRA-2018

## Appendix A. Supplementary data

Supplementary data to this article can be found online at https://doi.org/10.1016/j.ijbiomac.2020.06.290.

## References

[1] R.P. Berntsson, S.H. Smits, L. Schmitt, D.J. Slotboom, B. Poolman, A structural classification of substrate-binding proteins, FEBS Lett. 584 (12) (2010) 2606–2617.
[2] M.S. Luchansky, B.S. Der, S. D'Auria, G. Pocsfalvi, L. Iozzino, D. Marasco, J.D. Dattelbaum, Amino acid transport in thermophiles: characterization of an arginine-binding protein in Thermotoga maritima, Mol. BioSyst. 6 (1) (2010) 142–151.
[3] A. Scire, A. Marabotti, M. Staiano, L. Iozzino, M.S. Luchansky, B.S. Der, J.D. Dattelbaum, F. Tanfani, S. D'Auria, Amino acid transport in thermophiles: characterization of an arginine-binding protein in Thermotoga maritima. 2. Molecular organization and structural stability, Mol. BioSyst. 6 (4) (2010) 687–698.
[4] A. Ruggiero, J.D. Dattelbaum, A. Pennacchio, L. Iozzino, M. Staiano, M.S. Luchansky, B.S. Der, R. Berisio, S. D'Auria, L. Vitagliano, Crystallization and preliminary X-ray crystallographic analysis of ligand-free and arginine-bound forms of Thermotoga maritima arginine-binding protein, Acta Crystallogr. Sect. F Struct. Biol. Cryst. Commun. 67 (11) (2011) 1462–1465.
[5] A. Ausili, A. Pennacchio, M. Staiano, J.D. Dattelbaum, D. Fessas, A. Schiraldi, S. D'Auria, Amino acid transport in thermophiles: charcterization of an arginine-binding protein from Thermotoga maritima. 3. Conformational dynamics and stability, J. Photochem. Photobiol. B 118 (2013) 66–73.
[6] A. Ausili, M. Staiano, J. Dattelbaum, A. Varriale, A. Capo, S. D'Auria, Periplasmic binding proteins in thermophiles: characterization and potential application of an arginine-binding protein from Thermotoga maritima: a brief thermo-story, Life 3 (1) (2013) 149–160.
[7] L.J. Deacon, H. Billones, A.A. Galyean, T. Donaldson, A. Pennacchio, L. Iozzino, S. D'Auria, J.D. Dattelbaum, Tryptophan-scanning mutagenesis of the ligand binding pocket in Thermotoga maritima arginine-binding protein, Biochimie 99 (2014) 208–214.
[8] A. Ruggiero, J.D. Dattelbaum, M. Staiano, R. Berisio, S. D'Auria, L. Vitagliano, A loose domain swapping organization confers a remarkable stability to the dimeric structure of the arginine binding protein from Thermotoga maritima, PLoS One 9 (5) (2014), e96560. .
[9] N. Balasco, G. Smaldone, M. Vigorita, P. Del Vecchio, G. Graziano, A. Ruggiero, L. Vitagliano, The characterization of Thermotoga maritima arginine binding protein variants demonstrates that minimal local strains have an important impact on protein stability, Sci. Rep. 9 (1) (2019) 6617.
[10] G. Smaldone, N. Balasco, M. Vigorita, A. Ruggiero, S. Cozzolino, R. Berisio, P. Del Vecchio, G. Graziano, L. Vitagliano, Domain communication in Thermotoga maritima arginine binding protein unraveled through protein dissection, Int. J. Biol. Macromol. 119 (2018) 758–769.
[11] T. Donaldson, L. Iozzino, L.J. Deacon, H. Billones, A. Ausili, S. D'Auria, J.D. Dattelbaum, Engineering a switch-based biosensor for arginine using a Thermotoga maritima periplasmic binding protein, Anal. Biochem. 525 (2017) 60–66.
[12] M. Staiano, A. Pennacchio, A. Varriale, A. Capo, A. Majoli, C. Capacchione, S. D'Auria, Enzymes as sensors, Methods Enzymol. 589 (2017) 115–131.
[13] G. Smaldone, M. Vigorita, A. Ruggiero, N. Balasco, J.D. Dattelbaum, S. D'Auria, P. Del Vecchio, G. Graziano, L. Vitagliano, Proline 235 plays a key role in the regulation of the oligomeric states of Thermotoga maritima arginine binding protein, Biochim. Biophys. Acta 1864 (7) (2016) 814–824.
[14] G. Smaldone, A. Ruggiero, N. Balasco, A. Abuhammad, I. Autiero, D. Caruso, D. Esposito, G. Ferraro, E.L.M. Gelardi, M. Moreira, M. Quareshy, M. Romano, A. Saaret, I. Selvam, F. Squeglia, R. Troisi, L.M.J. Kroon-Batenburg, L. Esposito, R. Berisio, L. Vitagliano, The non-swapped monomeric structure of the arginine-binding protein from Thermotoga maritima, Acta Crystallogr F Struct Biol Commun 75 (Pt11) (2019) 707–713.
[15] G. Smaldone, R. Berisio, N. Balasco, S. D'Auria, L. Vitagliano, A. Ruggiero, Domain swapping dissection in Thermotoga maritima arginine binding protein: how structural flexibility may compensate destabilization, Biochim. Biophys. Acta 1866 (9) (2018) 952–962.
[16] M.M. Santoro, D.W. Bolen, Unfolding free energy changes determined by the linear extrapolation method. 1. Unfolding of phenylmethanesulfonyl α-chymotrypsin using different denaturants, Biochemistry 27 (1988) 8063–8068.
[17] C.N. Pace, F. Vajdos, L. Fee, G. Grimsley, T. Gray, How to measure and predict the molar absorption coefficient of a protein, Protein Sci. (11) (1995) 2411–2423.
[18] C.N. Pace, B.A. Shirley, J.A. Thomson, Measuring the conformational stability of a protein, Protein Structure: A Practical Approach, Oxford University Press, London 1989, pp. 311–330.
[19] P.L. Privalov, Stability of proteins: small globular proteins, Adv. Protein Chem. 33 (1979) 167–241.
[20] Y. Zhou, C.K. Hall, M. Karplus, The calorimetric criterion for a two-state process revisited, Protein Sci. 8 (5) (1999) 1064–1074.
[21] G.I. Makhatadze, P.L. Privalov, Protein interactions with urea and guanidinium chloride. A calorimetric study, J. Mol. Biol. 226 (1992) 491–505.
[22] Z. Otwinowski, W. Minor, Processing of X-ray diffraction data collected in oscillation mode, Methods Enzymol. 276 (1997) 307–326.
[23] A.J. McCoy, R.W. Grosse-Kunstleve, P.D. Adams, M.D. Winn, L.C. Storoni, R.J. Read, Phaser crystallographic software, J. Appl. Crystallogr. 40 (Pt4) (2007) 658–674.
[24] R.J. Morris, A. Perrakis, V.S. Lamzin, ARP/wARP and automatic interpretation of protein electron density maps, Methods Enzymol. 374 (2003) 229–244.
[25] G.N. Murshudov, A.A. Vagin, E.J. Dodson, Refinement of macromolecular structures by the maximum-likelihood method, Acta Crystallogr D Biol Crystallogr 53 (Pt3) (1997) 240–255.
[26] V. B. Chen, W. B. 3. Arendall, J. J. Headd, D. A. Keedy, R. M. Immormino, G. J. Kapral, L. W. Murray, J. S. Richardson, D. C. Richardson, MolProbity: all-atom structure validation for macromolecular crystallography, Acta Crystallogr D Biol Crystallogr 66 Pt 1 (2010) 12–21.
[27] R. Improta, L. Vitagliano, L. Esposito, Peptide bond distortions from planarity: new insights from quantum mechanical calculations and peptide/protein crystal structures, PLoS One 6 (9) (2011), e24533. .

[28] N. Balasco, L. Esposito, L. Vitagliano, Factors affecting the amplitude of the tau angle in proteins: a revisitation, Acta Crystallogr. Sect. D 73 (Pt7) (2017) 618–625.
[29] N. Balasco, L. Esposito, A.S. Thind, M.R. Guarracino, L. Vitagliano, Dissection of factors affecting the variability of the peptide bond geometry and planarity, Biomed. Res. Int. (2017) (2017) 2617629.
[30] L. Esposito, A. De Simone, A. Zagari, L. Vitagliano, Correlation between omega and psi dihedral angles in protein structures, J. Mol. Biol. 347 (3) (2005) 483–487.
[31] D. Van Der Spoel, E. Lindhal, B. Hess, G. Groenhof, A.E. Mark, H.J.C. Berendsen, GROMACS: fast, flexible, and free, J. Comput. Chem. 26 (2005) 1701–1718.
[32] T. Darden, D. York, L. Pedersen, Particle mesh Ewald: an N·log(N) method for Ewald sums in large systems, J. Chem. Phys. 98 (1993) 10089–10092.
[33] B. Hess, H. Bekker, H.J.C. Berendsen, J.G.E.M. Fraaije, LINCS: a linear constraint solver for molecular simulations, J. Comput. Chem. 18 (1997) 1463–1472.
[34] G. Bussi, D. Donadio, M. Parrinello, Canonical sampling through velocity rescaling, J. Chem. Phys. 126 (2007), 014101. .
[35] M. Parrinello, A. Rahman, Polymorphic transitions in single crystals: a new molecular dynamics method, J. Appl. Phys. 52 (1981) 7182–7190.
[36] A. Amadei, M.A. Ceruso, A. Di Nola, On the convergence of the conformational coordinates basis set obtained by the essential dynamics analysis of proteins' molecular dynamics simulations, Proteins 36 (1999) 419–424.
[37] A. Merlino, L. Vitagliano, M.A. Ceruso, L. Mazzarella, Subtle functional collective motions in pancreatic-like Ribonucleases: from ribonuclease A to angiogenin, Proteins 53 (1) (2003) 101–110.
[38] W. Humphrey, A. Dalke, K. Schulten, VMD: visual molecular dynamics, J. Mol. Graph. 14 (1) (1996) 33–38.
[39] R.A. Laskowski, M.B. Swindells, LigPlot+: multiple ligand-protein interaction diagrams for drug discovery, J. Chem. Inf. Model. 51 (10) (2011) 2778–2786.
[40] B. Mao, M. Pear, J. McCammon, F. Quiocho, Hinge-bending in L-arabinose-binding protein. The Venus' flytrap model, J. Biol. Chem. 257 (1982) 1131–1133.
[41] S. Cozzolino, R. Oliva, G. Graziano, P. Del Vecchio, Counteraction of denaturant-induced protein unfolding is a general proporty of stabilizing agents, Phys. Chem. Chem. Phys. 20 (2018) 29389–29398.
[42] G. Graziano, Contrasting the denaturing effect of guanidinium chloride with the stabilizing effect of guanidinium sulfate, Phys. Chem. Chem. Phys. 13 (2011) 12008–12014.
[43] T. Raskar, C.Y. Koh, S. Niebling, R.M. Kini, M.V. hosur, X-ray christallographic analysis of time-dependent binding of guanidine hydrochloride to HEWL: first steps during protein unfolding, Int. J. Biol. Macromol. 122 (2019) 903–913.
[44] M. Vazdar, J. Heyda, P.E. Mason, G. Tesei, C. Allolio, M. Lund, P. Jungwirth, Arginine "magic": guanidinium like-charge ion pairing from aqueous salts to cell penetrating peptides, Acc. Chem. Res. 51 (6) (2018) 1455–1464.
[45] Y. Tanaka, K. Tsumoto, M. Umetsu, T. Nakanishi, Y. Yasutake, N. Sakai, M. Yao, I. Tanaka, T. Arakawa, I. Kumagai, Structural evidence for guanidine-protein side chain interactions: crystal structure of CutA from Pyrococcus horikoshii in 3M guanidine hydrochloride, Biochem. Biophys. Res. Commun. 323 (1) (2004) 185–191.
[46] C.T. Armstrong, P.E. Mason, J.L. Anderson, C.E. Dempsey, Arginine side chain interactions and the role of arginine as a gating charge carrier in voltage sensitive ion channels, Sci. Rep. 6 (2016), 21759. .
[47] M.A. Neves, M. Yeager, R. Abagyan, Unusual arginine formations in protein function and assembly: rings, strings, and stacks, J. Phys. Chem. B 116 (23) (2012) 7006–7013.
[48] Z. Zhang, Z. Xu, Z. Yang, Y. Liu, J. Wang, Q. Shao, S. Li, Y. Lu, W. Zhu, The stabilization effect of dielectric constant and acidic amino acids on arginine–arginine (Arg–Arg) pairings: database survey and computational studies, J. Phys. Chem. B 117 (17) (2013) 4827–4835.
[49] D.B. Watlaufer, S.K. Malik, L. Stoller, R.L. Coffin, Nonpolar group participation in the denaturation of proteins by urea and guanidinium salts. Model compound studies, J. Am. Chem. Soc. 86 (3) (1964) 508–514.
[50] G. Graziano, Size and temperature dependence of hydrocarbon solubility in concentrated aqueous solutions of urea and guanidine hydrochloride, Can. J. Chem. 80 (4) (2002) 388–400.
[51] J.C. Ma, D.A. Dougherty, The cation−π interaction, Chem. Rev. 97 (5) (1997) 1303–1324.
[52] R. Breslow, T. Guo, Surface tension measurements show that chaotropic salting-in denaturants are not just water-structure breakers, PNAS 87 (1) (1990) 167–169.
[53] M.J. Parker, M. Lorch, R.B. Sessions, A.R. Clarke, Thermodynamic properties of transient intermediates and transition states in the folding of two contrasting protein structures, Biochemistry 37 (8) (1998) 2538–2545.